Asian Journal of Chemistry; Vol. 30, No. 7 (2018), 1503-1511
ASIAN JOURNAL OF CHEMISTRY
https://doi.org/10.14233/ajchem.2018.21193

Oxidation of Benzyl Alcohol in Slurry Phase Over Nanoporous ZrV_2O_7 Catalyst and Determination of Reaction Mechanism Using DFT

SHWETA KANUNGO JOSHI[1,*], N. SOHANI[1], S. KHARE[1], M.S. BATRA[2] and R. PRASAD[1]

[1]School of Chemical Sciences, Devi Ahilya Vishwavidyalaya, Indore-452 001, India
[2]Department of Chemistry, Khalsa College, Amritsar-143 002, India

*Corresponding author: E-mail: shwetakanungojoshi@gmail.com

Received: 22 December 2017; *Accepted*: 3 February 2018; *Published online*: 31 May 2018; AJC-18921

A process for high conversion of benzyl alcohol to benzaldehyde and benzoic acid over nanoporous ZrV_2O_7 is reported and mechanism is predicted by employing density functional theory (DFT). The reaction was carried out in slurry phase using air. Under optimum condition a maximum conversion of 93.89 % of benzyl alcohol was obtained. The catalyst was found to have 81.78 % selectivity for the benzoic acid. Mechanism for the reaction has been suggested from the analysis of reaction products and DFT modeling of the transition state. From the transition state modeling it is concluded that the reaction follows Mars-Van Krevelen type redox mechanism.

Keywords: Benzyl alcohol, Oxidation, ZrV_2O_7, DFT.

INTRODUCTION

There has been a considerable interest in the development of more economical and eco-friendly catalytic processes for the oxidation of alcohols to carbonyl compounds because of utility of aldehydes and acids in pharmaceuticals, dyes, perfumery and agro-chemical industries [1-5]. Conventional inorganic oxidants are costly, function in halogenated inorganic solvents and are environmental unfriendly [6-12]. Organic peroxides have also been used as oxidants for alcohol oxidation [13,14]. The use of hydrogen peroxide as an oxidant for organic reactions has a distinct advantage over other oxidizing agents as it produces water as the only by-product [15-18].

Although vapour phase processes are used for this transformation, control of selectivity towards partial oxidation to carbonyls and tendency towards combustion to CO_2 is the main disadvantage [19-22].

Liquid phase reactions employing phase transfer catalysts are associated with the problems of separation and reusability of catalyst [22]. Attempts have therefore been made to employing supported catalysts, which are free from these problems [23,24].

Catalytic oxidation of benzyl alcohol to benzaldehyde with air/oxygen over metal oxides, supported metal oxides and mixed metal oxides offers advantages over the homogenous catalysis in terms of the ease in the separation of product and reusability [25,26].

Solution combustion is a new process for rapid synthesis of porous oxides, mixed oxides and supported metal oxides [27,28]. In this process, slurry consisting of nitrates of the precursors is mixed with a fuel like urea/citric acid and heated for few minutes in a microwave oven till a solid gel is formed. The gel is ignited in a muffle furnace to get the oxide materials.

To the best of our knowledge there is no report on the mechanism of oxidation of benzyl alcohol over ZrV_2O_7 catalyst employing any quantum mechanical approach. Density functional theory is the latest approach in quantum mechanics to model reaction pathways and transition states in chemical reactions.

In the present manuscript we report liquid phase air oxidation of benzyl alcohol over zirconium vanadate catalyst prepared by solution combustion method with the objectives of (1) optimizing the process conditions for maximum yield to the carbonyl compound (2) to model the transition states of the reaction by DFT theory (3) to compute the activation energy of the reaction and (4) to predict the mechanism of the reaction.

EXPERIMENTAL

ZrV_2O_7 catalyst was prepared by solution combustion method. Salts of zirconium and vanadium were used for the preparation of the catalyst. Citric acid was used as a fuel. In a typical preparation, 12.32 g of $Zr(NO_2)$, 0.6460 g of $NH_4(VO_3)$ and 25.92 g of citric acid were mixed in minimum quantity of water to make a slurry. The slurry was heated over a hot plate where it swells into a gel. The resultant product was grinded and kept in the muffle furnace for the calcination at 550 °C for 4 h. Yellow green product is obtained which is further grinded in order to prepare a fine powder.

General procedure: Reaction was carried out in a three necked borosil flask equipped with thermometer pocket, reflux condenser and air feed system. A manometer was used to meter the flow rate of air. Three necked flask was kept in a water bath whose temperature was regulated with the help of controlled power supply. In a typical run, about 1g of benzyl alcohol was charged to the reactor along with solvent (dichloromethane) and heated. Air was bubbled to the reaction mixture and the system was allowed to reflux. After completion of the reaction, the reactor was cooled and catalyst was filtered. The filtered reaction mixture was distilled to separate the solvent, reactant and products.

All the DFT calculations for dehydrogenation of benzyl alcohol over the catalyst were carried out employing Gaussian 09W suite, using B3LYP functionals to describe electron exchange and correlation and Lanl2dz basis set to find the optimized geometries of reactants, products and transition states [29,30]. For transition state calculation QST2/QST3 keywords have been used [31]. At many places the optimization of transition state was achieved directly also [32]. Unfortunately, it is not a common case. Many times optimized geometries are still not good enough to predict the transition state geometry. In these cases, various techniques such as potential surface scan and linear synchronous transit (LST) methods have been applied to get close to a transition state. Vibrational frequencies were calculated for the optimized geometries to identify the nature of the reactant or product (no imaginary frequency) and TS (one imaginary frequency). The enthalpy and the activation energies were calculated at the reaction temperature as described by Ochterski [33]. For large and less well behaved species, optimization can be achieved by lowering the cutoff value with the help of SCF option provided in Gaussian.

Convergence has been considered to be achieved when forces on the atoms become less than the cutoff value. The adsorption energy (E_{ads}) was calculated as:

$$E_{ads} = E_{(adsorbate - substrate)} - (E_{adsorbate} + E_{substrate})$$

where $E_{(adsorbate - substrate)}$ is the total energy of the adsorbate–substrate system in the equilibrium state and $E_{substrate}$ and $E_{adsorbate}$ are the energies of isolated substrate and adsorbate, respectively [34,35]. By this definition, a negative value of E_{ads} corresponds to an exothermic process.

Geometry optimization for all the structures was performed. A comparison of some of the geometrical parameters from optimized and crystallographic structures was performed. The DFT results indicated that the optimized distances and angles in the model were in good agreement with the experimental values [36].

Detection method: Catalyst was characterized by X-ray diffraction (XRD) and Raman analysis. XRD in the 2θ range 0-90° was performed over Rigaku X-ray powder diffractometer equipped with graphite-crystal monochromator employing CuK_α radiation of wavelength 1.5406 Å as a source. The average particle size was calculated from (111) diffraction peak using Scherer's equation:

$$D = 0.9\lambda/(\beta\cos\theta)$$

where D is the average crystallite size in nm, λ is the wavelength of source X-ray (0.154 nm), β (in radian) is the full peak width at half maximum. Raman spectrum of the sample in the range 50-4000 cm^{-1} was recorded over a Labram HR800 micro Raman spectrometer using Labspec software. An Ar^+ source with the wavelength 2.53 eV was used as a source.

The product containing reaction mixture was analyzed with the help of a chemito1000 Chromatograph using SE-30 column and FID detector.

RESULTS AND DISCUSSION

X-ray diffraction analysis: Powder XRD pattern of the prepared nanoparticles was recorded in order to explore structural features of zirconium supported mesoporous vanadium materials. Fig. 1 depicts XRD patterns, which confirms that the vanadium ions have occupied the zirconium ions at their lattice positions with high dispersion of vanadium ions on zirconium oxide surface [37]. A sharp peak appeared at 30.23°, which can be ascribed to tetragonal phase of ZrO_2. The average particle size was calculated from (111) diffraction peak using Scherer's equation [38]. The average particle size found within the range of 20-26 nm.

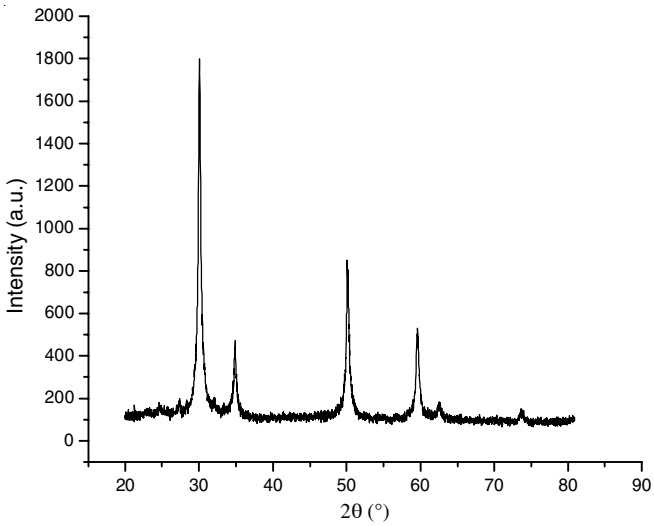

Fig. 1. XRD pattern of ZrV_2O_7 nanoparticles

Raman analysis: The bands appeared at 330, 482 and 639 cm^{-1} are assigned to ZrO_2. The low frequency bands appeared at 144.8, 175.9 and 188 cm^{-1} are assigned to lattice vibrations. Bands appeared at 1372 and 1597 cm^{-1} can be attributed to bending modes of water. The band appeared at 1042 cm^{-1} in the Raman spectrum can be ascribed to stretching vibration of short V=O bond. A strong Raman band at 996 cm^{-1} is generally assigned to V=O stretching mode of bulk V_2O_5 [39]. Weak intensity of this band in the present recording suggests low concentration of bulk V_2O_5 (Fig. 2).

Catalyst structure and its optimization: The structure of catalyst was optimized and the obtained bond lengths and bond angles were compared with the reported ones. For geometry optimization of the catalyst, an octahedral environment for zirconium and tetrahedral environment for vanadium was assumed. The calculated bond lengths for V=O (vanadyl group), V-O bridging *viz.*, $V\text{-}O_{Zr}$ and $V\text{-}O_V$ as 1.59, 1.70 and 1.77 Å, respectively compared well with the reported values of 1.66, 1.68 and 1.75 Å, respectively. The calculated bond length for

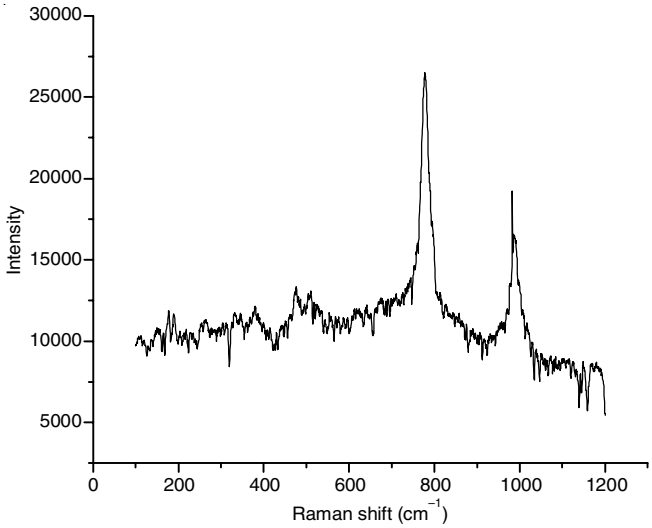

Fig. 2. Raman spectrum of the ZrV_2O_7 nanoparticles

Zr-O was 2.08 Å (Experimental value- 2.06 Å) while the V-O-V and Zr-O-V bond angles were 165.8° (Experimental value- 166.2°) and 153.4° (Experimental value- 154.7°), respectively.

Activity of the catalyst

Effect of catalyst loading on the performance of ZrV_2O_7 catalyst: Effect of catalyst loading on the performance of ZrV_2O_7 catalyst was studied at constant temperature of 80 °C and constant flow rate of air. Best performance was achieved at a catalyst loading of 5 % of the alcohol was fed. Conversion increased with catalyst loading and attempted towards a constant. Conversion to benzoic acid constantly increased with catalyst loading. On the other hand conversion to benzaldehyde increased in the beginning but dropped above 2 % of catalyst loading (Fig. 3). This led to an increase in the selectivity towards benzoic acid.

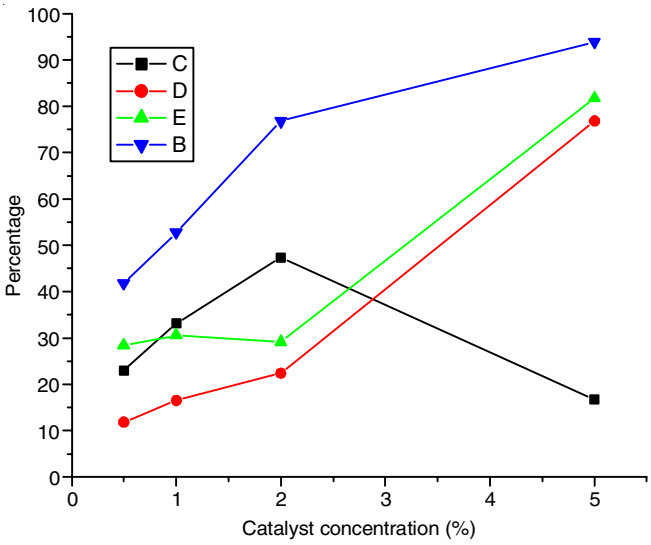

Fig. 3. Effect of catalyst loading on the performance of ZrV_2O_7 catalyst in the oxidation of benzyl alcohol. B = Conversion, C = Benzaldehyde, D = Benzoic acid, E = Selectivity for benzoic acid. (Time of run = 8 h, temperature = 80 °C, air flow rate =30 L h^{-1})

Effect of temperature on the performance of ZrV_2O_7 catalyst: Effect of temperature on the performance parameters such as conversion, yield and selectivity of products is graphically shown in Fig. 4. The study suggests that there is an increase in the conversion of benzyl alcohol, yield and selectivity of benzoic acid with increase in temperature. However yield of benzaldehyde decreased with increasing temperature.

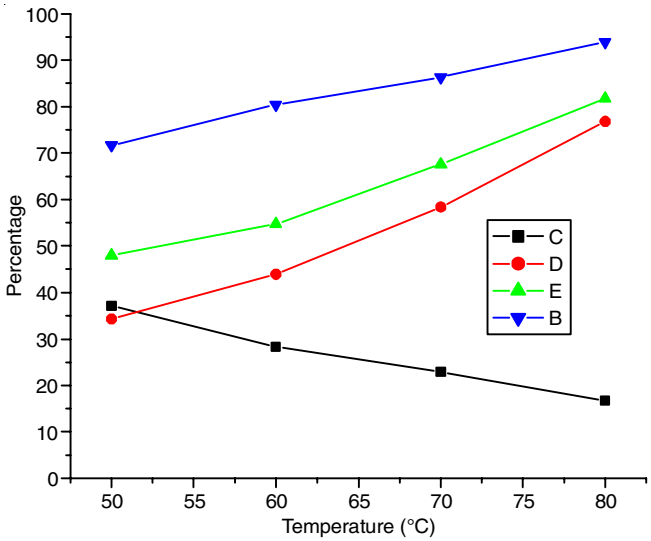

Fig. 4. Effect of temperature on the performance of ZrV_2O_7 catalyst in the oxidation of benzyl alcohol. B = Conversion, C = Benzaldehyde, D = Benzoic acid, E = Selectivity for benzoic acid (Time of run = 8 h, benzyl alcohol feed rate = 1 g h^{-1}, Air flow rate = 30 L h^{-1})

Effect of time on stream on the performance of ZrV_2O_7 catalyst: This study was performed to find the regeneration time of the catalyst. The findings are presented graphically in Fig. 5. It can be seen that conversion as well as yield and selectivity of benzoic acid increased with increasing time on stream. The catalyst activity was found fairly well up to 8 h. After 2 h conversion benzaldehyde became almost constant.

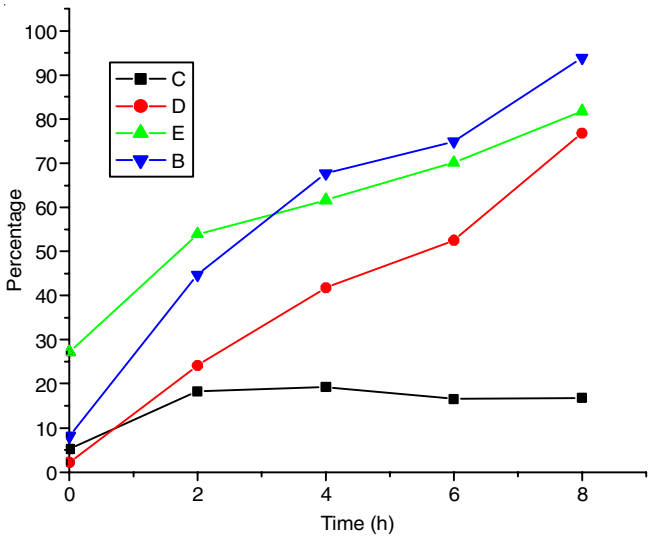

Fig. 5. Effect of time stream on the performance of ZrV_2O_7 catalyst in the oxidation of benzyl alcohol. B = Conversion, C = Benzaldehyde, D = Benzoic acid, E = Selectivity for benzoic acid. (Temperature 80 °C, air flow rate = 30 L h^{-1})

DFT calculations

Molecular adsorption of benzyl alcohol: The adsorption of benzyl alcohol over ZrV_2O_7 is shown in Fig. 6.

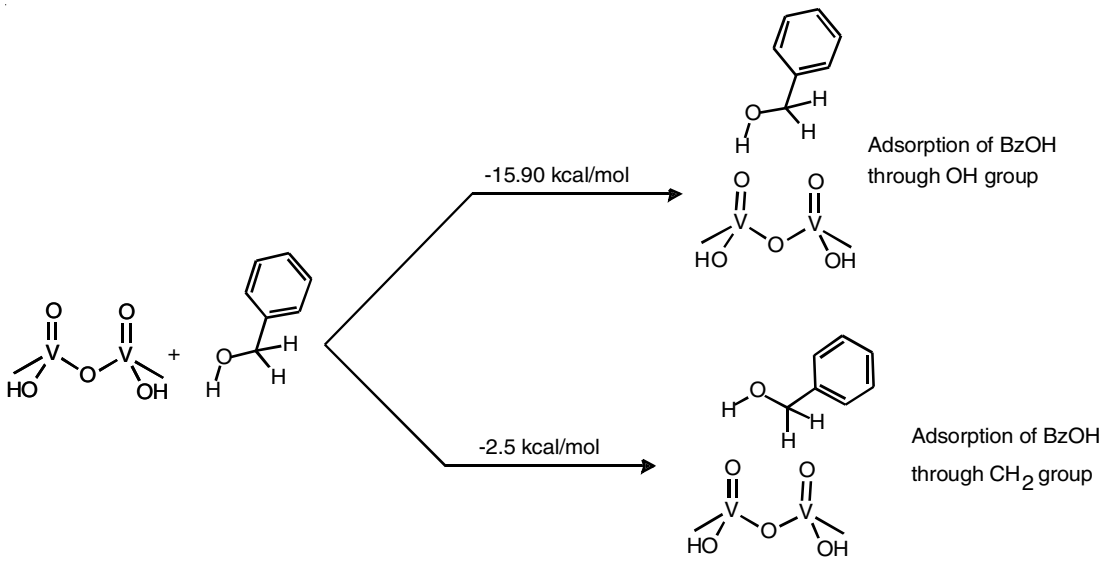

Fig. 6. Molecular adsorption of benzyl alcohol

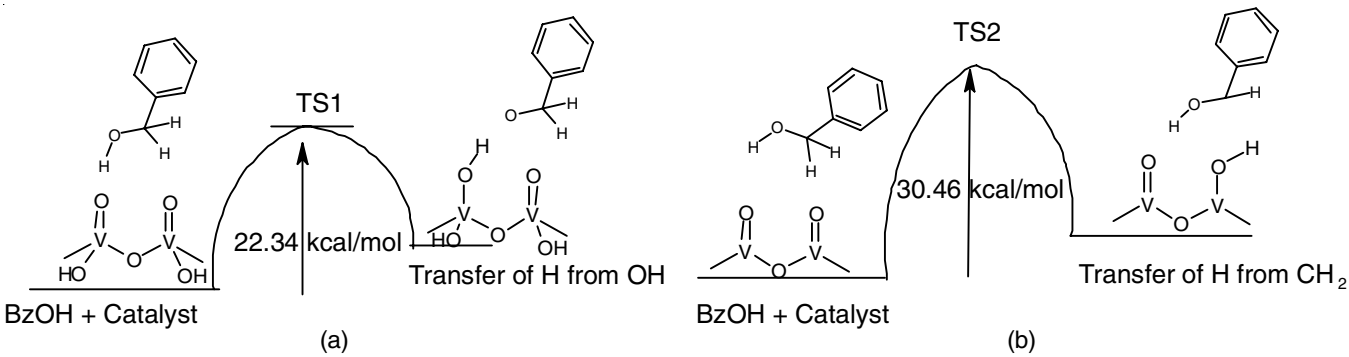

Fig. 7. Schematic PES diagram for hydrogen abstraction by the catalyst from (a) OH group (b) CH_2 group of benzyl alcohol

The adsorption over the catalyst surface may involve interactions between OH group or methylene group of the alcohol and the V=O of the catalyst. Calculations revealed higher heat of adsorption through OH group (-15.90 kcal mol^{-1}) compared to the adsorption through methylene group (-2.5 kcal mol^{-1}).

Abstraction of first hydrogen from benzyl alcohol: DFT calculations on the dehydrogenation of benzyl alcohol have been performed for the abstraction of hydrogen from both O-H and C-H bonds. The potential energy surface (PES) diagram for H atom abstraction from OH and CH_2 groups is shown in Fig. 7.

The activation energy for H abstraction from OH group is 22.34 kcal mol^{-1} while from methylene group is 30.46 kcal mol^{-1} suggesting that the former abstraction is taking place in the first step producing a benzyl oxide ion. The optimized structures of reactant model for H abstraction from OH or CH_2 groups of benzyl alcohol are shown in Fig. 8.

The O-H bond length of 0.987 Å in the intermediate (Fig. 8a) is very close to the normal bond length in alcohol. In most of the literature reports interactions between the initially formed oxide ion and metal of the catalyst have been reported. For such interactions to take place in case of zirconium vanadate catalyst, the benzyl oxide ion will have to go closer to the vanadium metal, which seems to be sterically hindered. The optimized geometries indicate that it prefers to stay near the transferred hydrogen, *i.e.*, the newly formed O-H group with a distance of 1.857 Å (Fig. 8a).

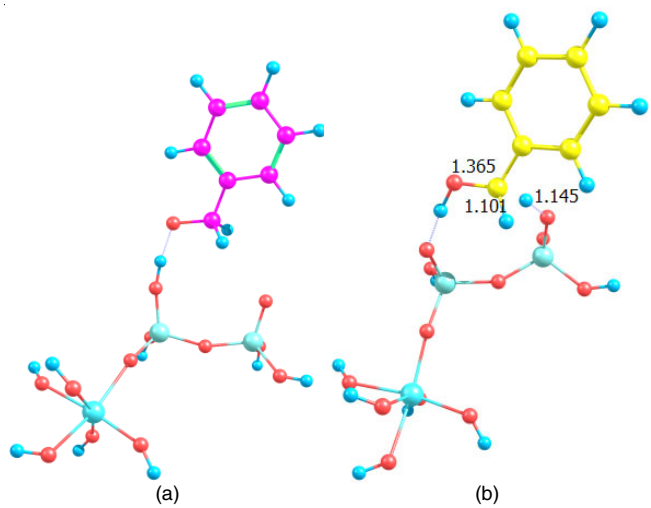

Fig. 8. Hydrogen abstraction by the catalyst from (a) OH and (b) CH_2 groups of benzyl alcohol

The T.S. structures for both possibilities are shown in Fig. 9(a) and 9(b). The BzO···H and VO···H bond lengths in T.S. structure (Fig. 9a) are found to be 1.71 Å and 1.35 Å, respectively while for the T.S. structure for H abstraction from methylene

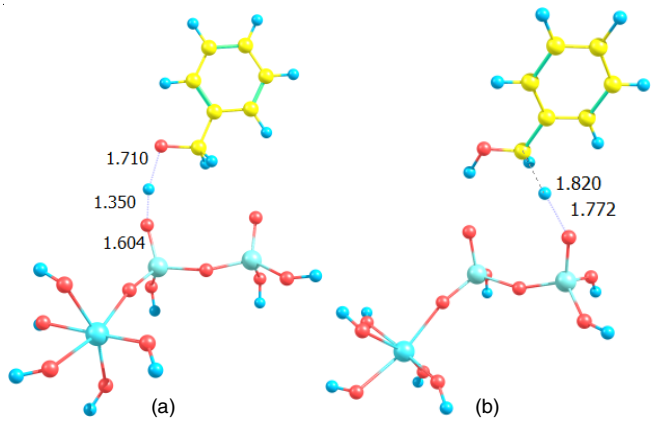

Fig. 9. T.S. structure for hydrogen abstraction by the catalyst from (a) OH or (b) CH_2 groups of benzyl alcohol

group the C-H and O-H bond lengths are 1.82 Å and 1.77 Å, respectively. The T.S. calculations indicate one imaginary frequency for transfer of H, which is calculated at 1852.6*i* cm^{-1}.

Abstraction of second hydrogen from benzyl alcohol: The removal of second H from methylene group of the benzyl oxide intermediate to produce benzaldehyde is the rate determining step for the oxidative dehydrogenation of benzyl alcohol. It may involve the vanadium site V_1 or V_2. The activation energy for the abstraction of second hydrogen by V_1 is 59.8 kcal mol^{-1} and the translational frequency is at 1070.26*i* cm^{-1}. The structure of the intermediate is shown in Fig. 10. Similar abstraction of second hydrogen by V_2 requires higher activation energy 93.25 kcal mol^{-1} and the translational frequency is at 989.8*i* cm^{-1}. Thus transfer of second hydrogen to V_1 is more favourable than to V_2. The T.S. structures for these two possibilities are shown in Figs. 10 and 11.

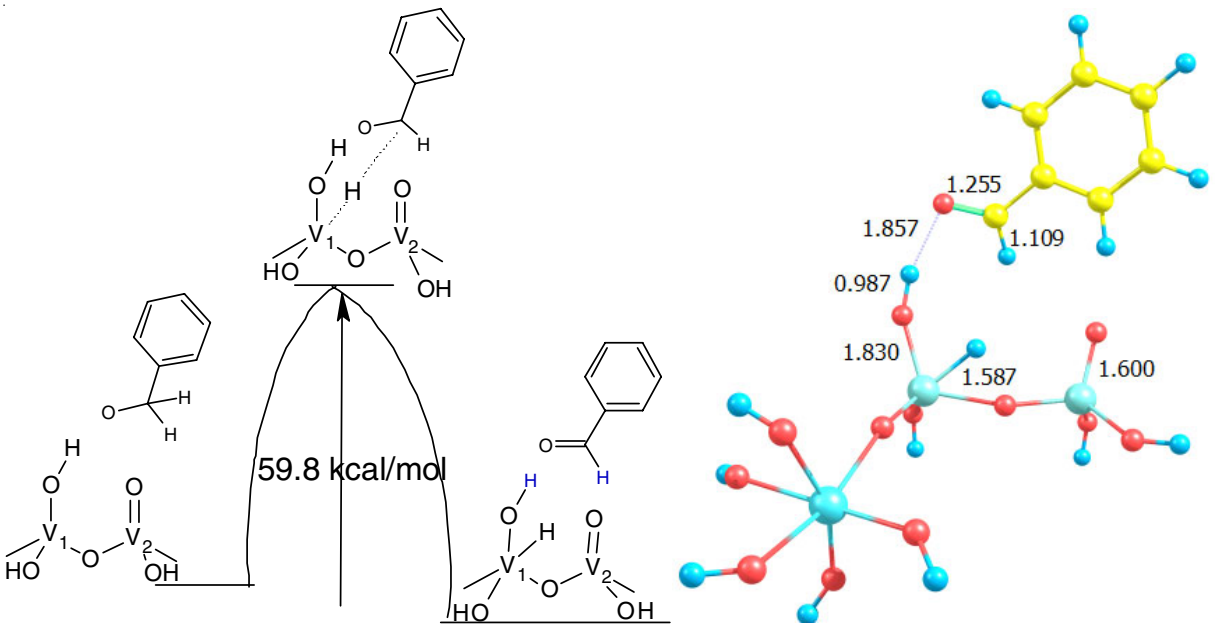

Fig. 10. Hydrogen transfer to V_1 of catalyst from CH_2 group of benzyloxy ion

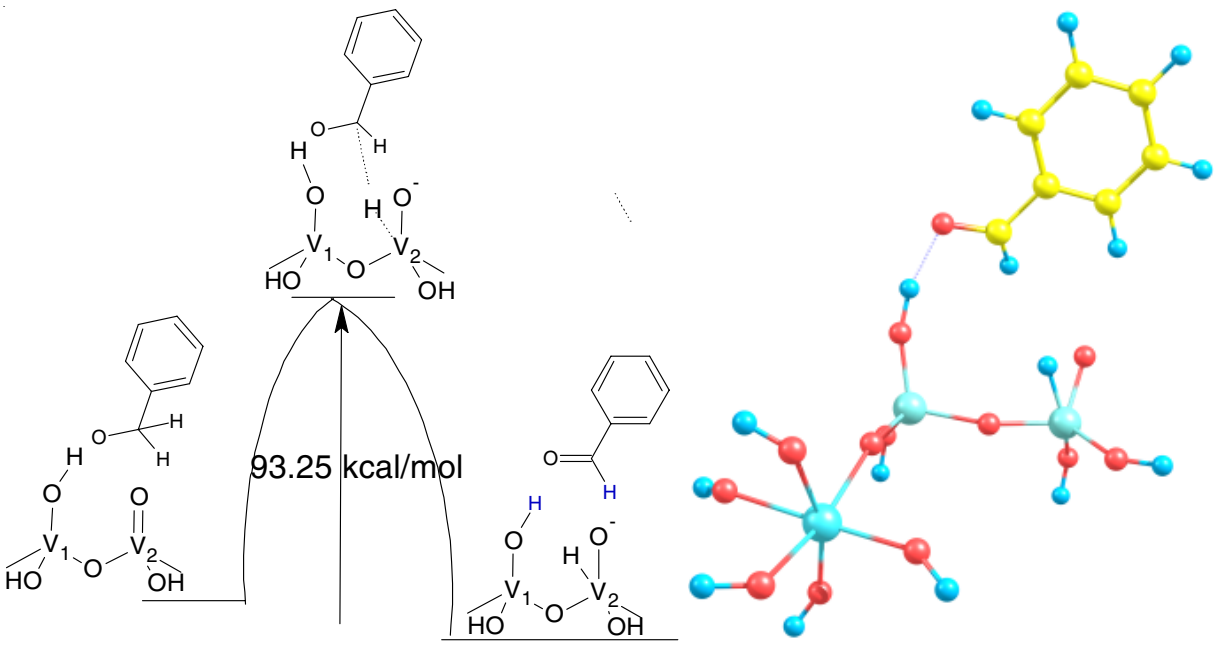

Fig. 11. Hydrogen transfer to V_2 of catalyst from CH_2 group of benzyloxy ion

Transfer of V-H to nearby oxygen atoms: The structure formed in Fig. 10. With V-H bond is not very stable and transfers its hydrogen to attached OH group or the nearby oxygen atoms O2 or O3 to form V-OH. On the basis of oxygen sites involved, we can describe the whole mechanism into three categories: Mechanism involving O1 site; Mechanism involving O2 site and Mechanism involving O3 site.

Mechanism involving O1 site: If transfer of H from V-H involves the interaction with O1 of V-OH moiety, it leads to the formation of product benzaldehyde and water molecule, which later on get desorbed and give rise to a vacancy at vanadium site. The T.S. has been calculated and the activation energy was found to be 6.9 kcal mol^{-1} with a translational frequency at 828.4*i* cm^{-1}. The T.S. structure is shown in Fig. 12b.

Mechanism involving O2 site: If transfer of H from V-H involves the interaction with nearby bridged oxygen O2 of VOV moiety, it leads to the formation of product benzaldehyde and V-O-H group (Fig. 13) in the intermediate species, the later in subsequent steps regenerates the catalyst. In the T.S. lengthening of V-H bond takes place thus bringing it closer to the oxygen atom. The T.S. structure for this possibility is shown in Fig. 13b.

Mechanism involving O3 site: If transfer of H from V-H involves the interaction with nearby oxygen O3 of V=O moiety, it leads to the formation of product benzaldehyde and V-O-H

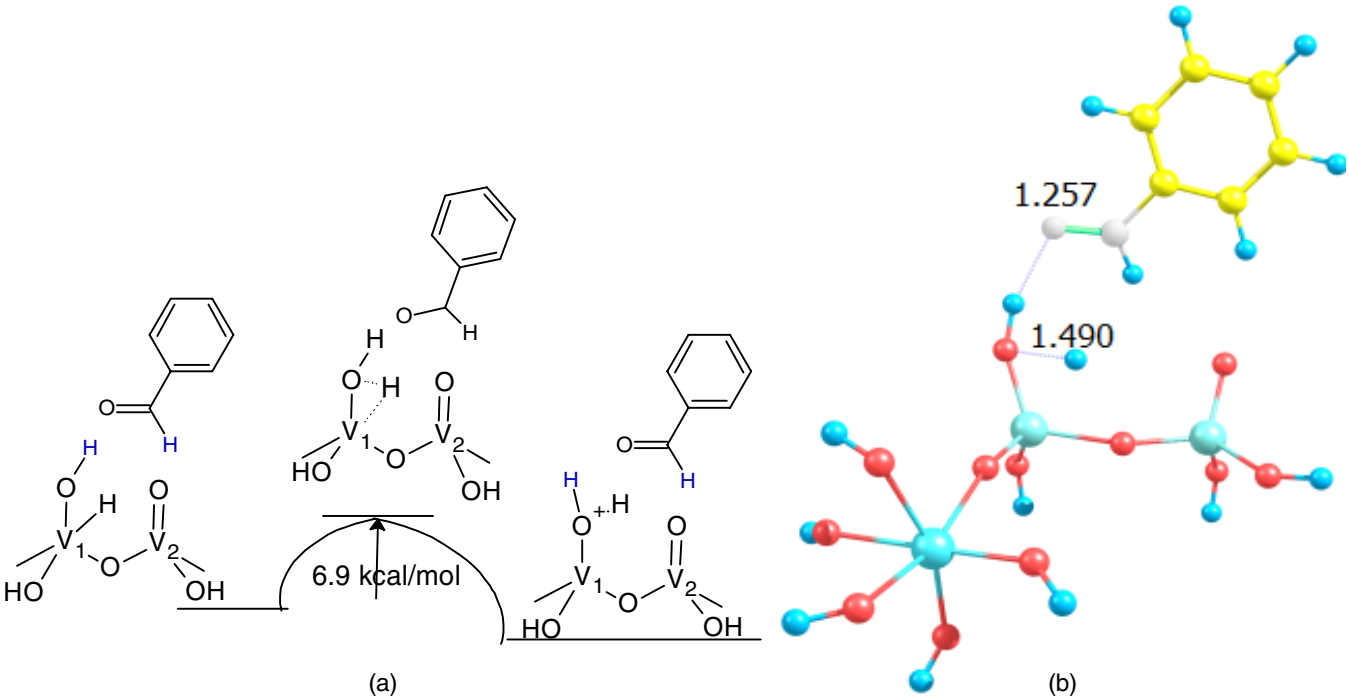

Fig. 12. (a) The PES diagram and (b) T.S. structure for hydrogen transfer from V_1-H to OH group

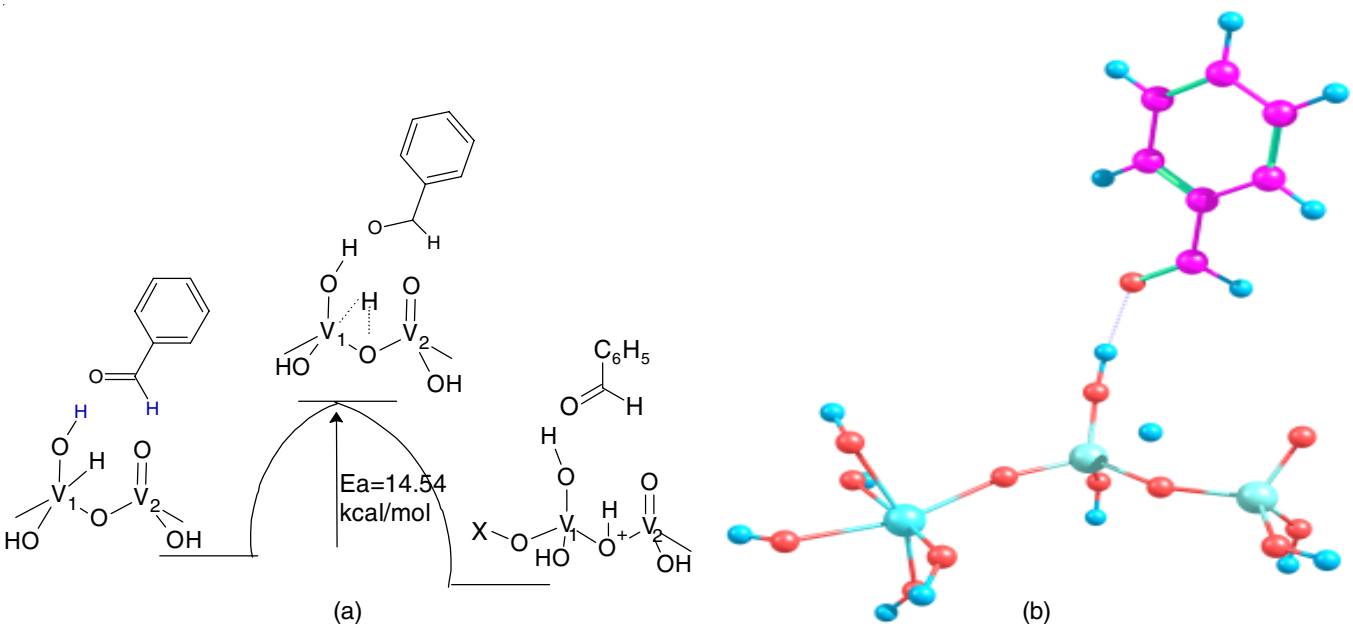

Fig. 13(a). The PES diagram and (b) T.S. structure for hydrogen transfer from V_1-H to O2

group in the intermediate species, the later in subsequent steps regenerates the catalyst. In the T.S. lengthening of V-H bond takes place thus bringing it closer to the oxygen atom. The T.S. structure for this possibility is shown in Fig. 14.

Formation and desorption of product from reaction site: From the aforesaid discussion it can be concluded that oxidative dehydrogenation of benzyl alcohol over the catalyst surface involves adsorption of the alcohol over the catalyst surface, through its OH group. This is followed by abstraction of hydrogen atom from either OH or CH_2 group of $PhCH_2OH$ (Paths A and B). Abstraction of OH hydrogen atom (Path B) requires much lower energy than that from the methylene (CH_2) group. The intermediate thus formed loses the second hydrogen atom to the nearby vanadium atom, V_1 or V_2 to produce benzaldehyde (Paths C and D). Transfer of H to V1 (Path D) is a lower energy process (Fig. 15).

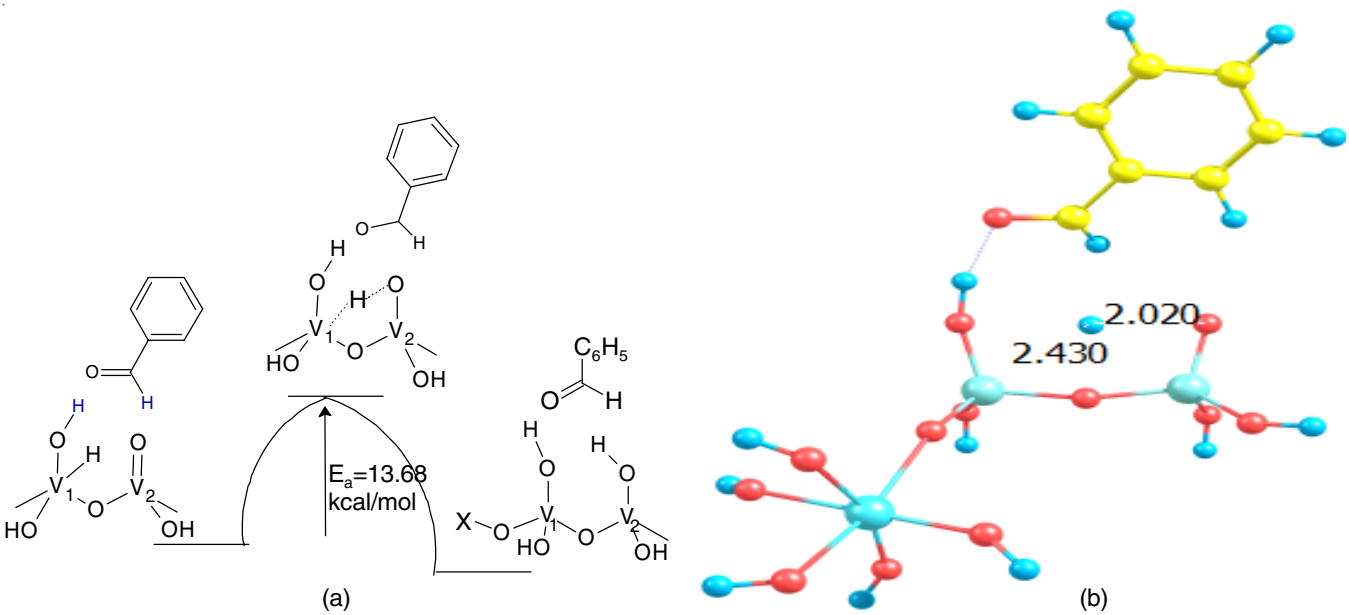

Fig. 14. (a) the PES diagram and (b) T.S. structure for hydrogen transfer from V_1-H to O3

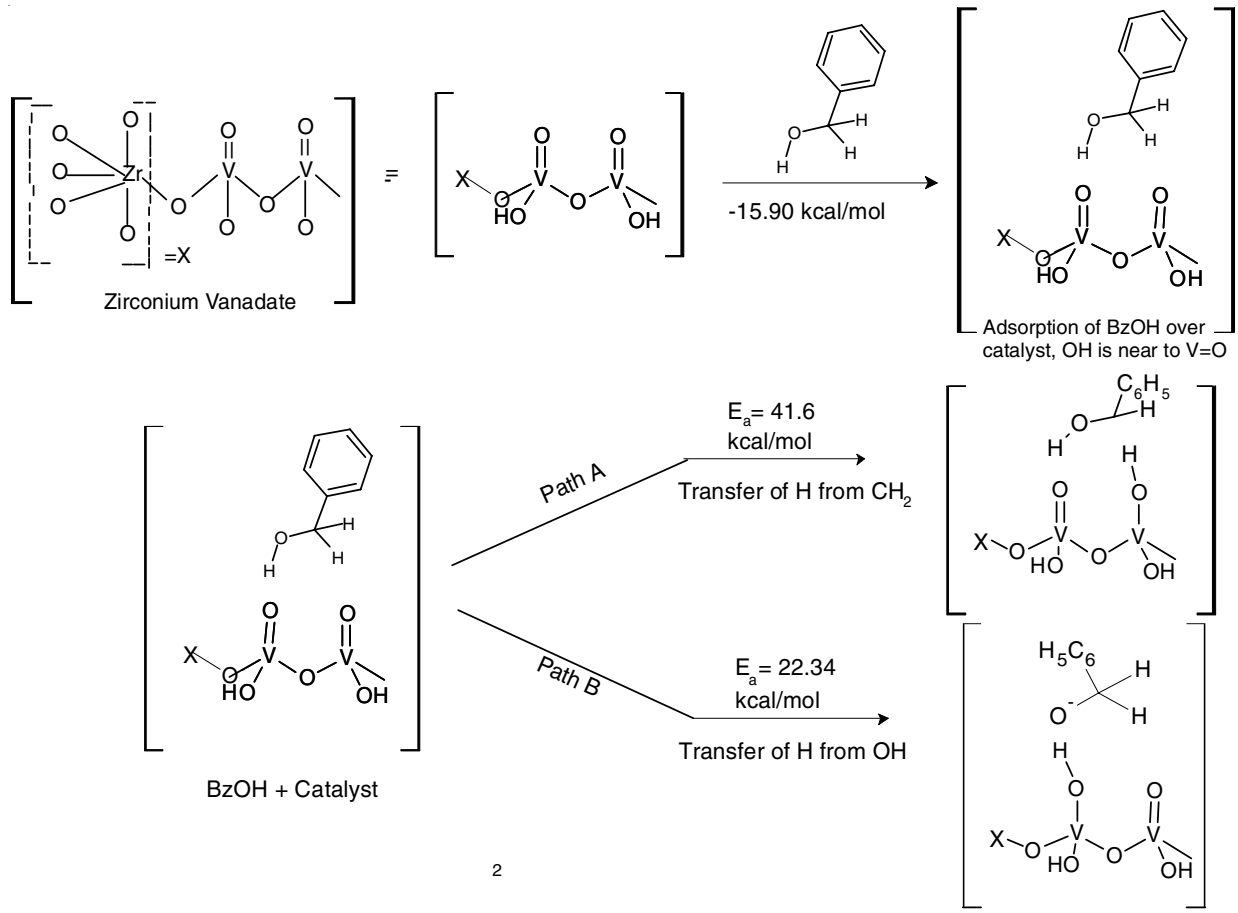

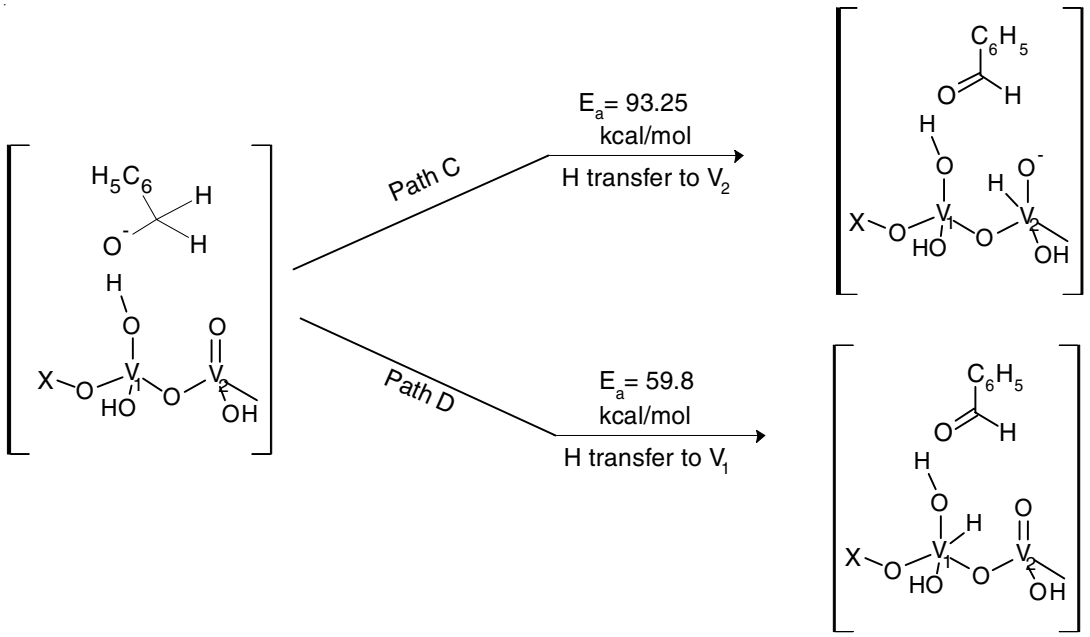

Fig. 15. Mechanism of dehydrogenation of benzyl alcohol over zirconium vanadate catalyst

Catalyst regeneration: The product benzaldehyde formed undergoes desorption and the catalyst is regenerated by three possible pathways namely transfer of H from V-H to OH of the attached group (Path E), O atom of the bridged V-O-V group (Path F) or of nearby V=O group (Path G). The activation energies for these three steps are 6.9, 14.54 and 13.68 kcal mol^{-1}, respectively. The steps are depicted in Fig. 16.

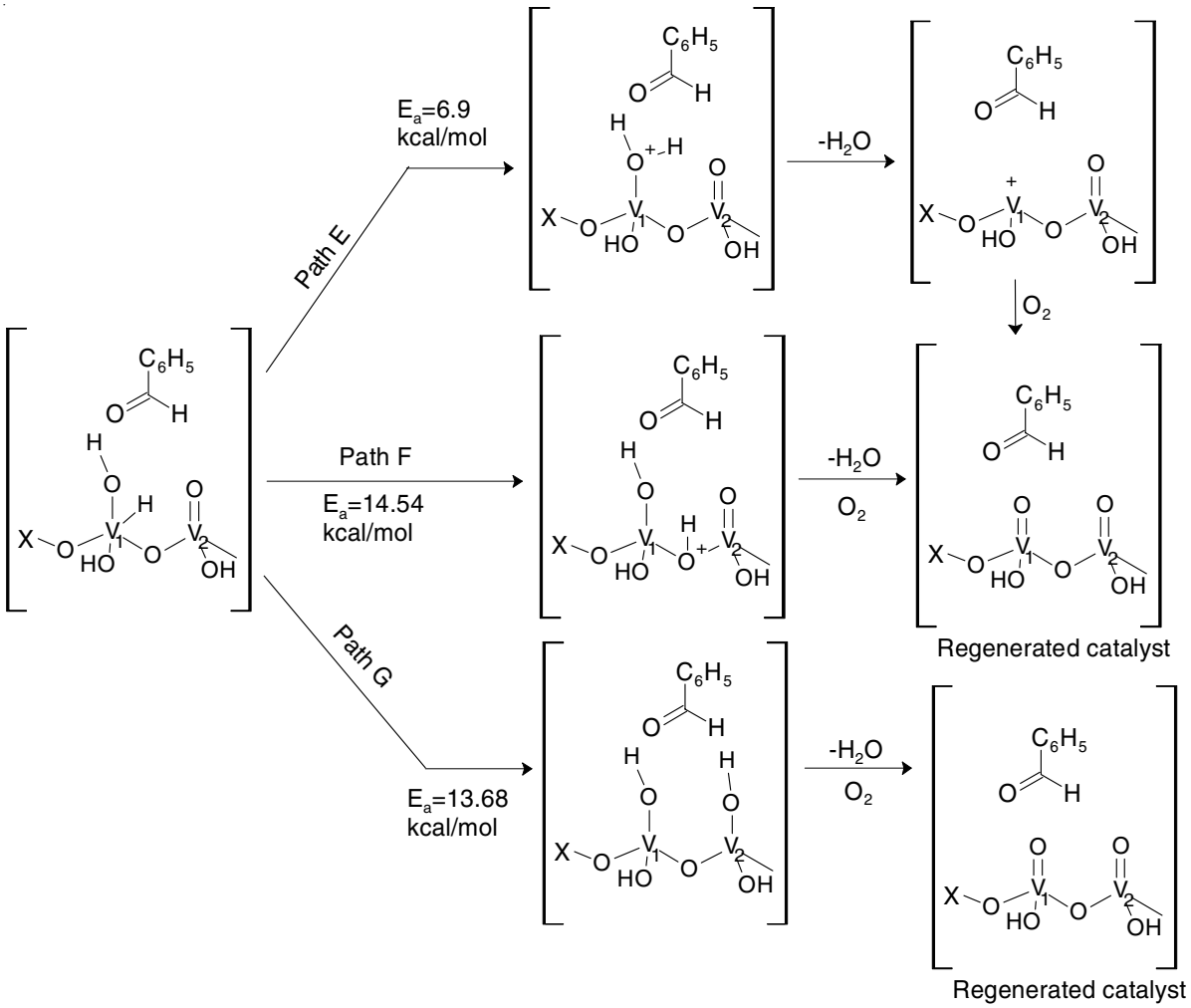

Fig. 16. Possible steps for regeneration of catalyst

Conclusion

A green process for synthesis of carbonyl compounds (benzoic acid/benzaldehyde) has been developed by the oxidation of benzyl alcohol employing air as an oxidizing agent. The reaction was catalyzed by nanoporous ZrV_2O_7 catalyst, prepared through solution combustion method. This mixed metal oxide shown to have a good selectivity (81.78 % for the benzoic acid) towards the particular oxidation process with a maximum conversion of 93.89 % of benzyl alcohol at moderate reaction conditions. Mechanism of the reaction was predicted with the help of density functional theory calculations. The reaction starts with adsorption of alcohol over the catalyst, followed by the abstraction of hydrogen from OH group of alcohol by vanadyl oxygen giving rise to benzyl oxide type intermediate. The intermediate then loses hydrogen from the methylene group with the help of nearby vanadium atom to produce benzaldehyde. The minimum energy paths for abstraction of both hydrogen atoms from benzyl alcohol have been computed. The activation energies for different paths and geometries of all the transition states are reported.

Efficiency of ZrV_2O_7 catalyst towards the particular oxidation reaction provides a green and safe option for the synthesis of carbonyl compounds. Its application may be extended for the large scale production of these compounds.

ACKNOWLEDGEMENTS

The authors are thankful to UGC-DAE-CSR, Indore, India for spectral analysis. The authors are also grateful to IPCA Laboratories, Indore, India for GLC recordings.

REFERENCES

1. R.A. Sheldon and J.K. Kochi, Metal-Catalyzed Oxidations of Organic Compounds: Mechanistic Principles and Synthetic Methodology Including Biochemical Processes, Academic Press: New York (1981).
2. S. Caron, R.W. Dugger, S.G. Ruggeri, J.A. Ragan and D.H.B. Ripin, *Chem. Rev.*, **106**, 2943 (2006); https://doi.org/10.1021/cr040679f.
3. M. Hudlicky, Oxidations in Organic Chemistry, ACS Monograph Series, ACS: Washington, DC (1990).
4. J. E. Bäckvall, Modern Oxidation Methods, John Wiley & Sons (2011).
5. T. Punniyamurthy, S. Velusamy and J. Iqbal, *Chem. Rev.*, **105**, 2329 (2005); https://doi.org/10.1021/cr050523v.
6. F.M. Menger and C. Lee, *Tetrahedron Lett.*, **22**, 1655 (1981); https://doi.org/10.1016/S0040-4039(01)90402-2.
7. J. Muzart, *Chem. Rev.*, **92**, 113 (1992); https://doi.org/10.1021/cr00009a005.
8. G. Cainelli and G. Cardillo, Chromium Oxidants in Organic Chemistry, Springer: Berlin (1984).
9. S.V. Ley and A. Madin, eds.: B.M. Trost and I. Fleming, Comprehensive Organic Synthesis, Pergamon Press, Oxford, UK, vol. 7, p. 291 (1991).
10. T.V. Lee, eds.: B.M. Trost and I. Fleming, Comprehensive Organic Synthesis, Pergamon Press, Oxford, UK, vol. 7, p. 291 (1991).
11. W.P. Griffith, *Chem. Soc. Rev.*, **21**, 179 (1992); https://doi.org/10.1039/cs9922100179.
12. D.B. Dess and J.C. Martin, *J. Org. Chem.*, **48**, 4155 (1983); https://doi.org/10.1021/jo00170a070.
13. M.G. Buonomenna and E. Drioli, *J. Appl. Catal. B*, **79**, 35 (2008); https://doi.org/10.1016/j.apcatb.2007.10.003.
14. V.R. Choudhary, D.K. Dumbre and S.K. Bhargava, *Ind. Eng. Chem. Res.*, **48**, 9471 (2009); https://doi.org/10.1021/ie801883d.
15. G. Strukul, Catalytic Oxidations with Hydrogen Peroxide as Oxidant, Kluwer Academic Publishers: Netherlands (1992).
16. Y. He, X. Ma and M. Lu, *ARKIVOC*, 187 (2012); https://doi.org/10.3998/ark.5550190.0013.817.
17. F. Adam and O. Wan-Ting, *J. Phy. Sci. (Malaysia)*, **24**, 1 (2013).
18. S. Masoudian and H. Yahyaei, *Indian J. Chem.*, **50A**, 1002 (2011).
19. A. Kumar, V.P. Kumar, B.P. Kumar, V. Vishwanathan and K.V.R. Chary, *Catal. Lett.*, **144**, 1450 (2014); https://doi.org/10.1007/s10562-014-1285-6.
20. A. Kumar, B. Sreedhar and K.V.R. Chary, *J. Nanosci. Nanotechnol.*, **15**, 1714 (2015); https://doi.org/10.1166/jnn.2015.9022.
21. C. Srinivasan and B. Viswanathan, *Indian J. Chem.*, **41B**, 1349 (2002).
22. K. Bijudas, P. Bashpa, K.P.A. Nasrin, K. Krishnapriya and R. Krishnan, *J. Chem. Sci. Rev. Lett.*, **3**, 123 (2014).
23. J.S. Rebello, S.P. Naik and J.B. Fernandes, *Indian J. Chem.*, **43B**, 1676 (2004).
24. V.R. Choudhary, R. Jha and P. Jana, *Green Chem.*, **9**, 267 (2007); https://doi.org/10.1039/b608304h.
25. M. Ilyas and M. Sadiq, *Chem. Eng. Technol.*, **30**, 1391 (2007); https://doi.org/10.1002/ceat.200700072.
26. R. Sumathi, K. Johnson, B. Viswanathan and T.K. Varadarajan, *J. Appl. Catal. A*, **172**, 15 (1998); https://doi.org/10.1016/S0926-860X(98)00119-7.
27. S.T. Aruna and A.S. Mukasyan, *Curr. Opin. Solid State Mater. Sci.*, **12**, 44 (2008); https://doi.org/10.1016/j.cossms.2008.12.002.
28. K. Sivaranjani, A. Verma and C.S. Gopinath, *Green Chem.*, **14**, 461 (2012); https://doi.org/10.1039/C1GC15907K.
29. M.J. Frisch, G.W. Trucks, H.B. Schlegel, G.E. Scuseria, M.A. Robb, J.R. Cheeseman, G. Scalmani, V. Barone, B. Mennucci, G.A. Petersson, H. Nakatsuji, M. Caricato, X. Li, H.P. Hratchian, A.F. Izmaylov, J. Bloino, G. Zheng, J.L. Sonnenberg, M. Hada, M. Ehara, K. Toyota, R. Fukuda, J. Hasegawa, M. Ishida, T. Nakajima, Y. Honda, O. Kitao, V.H.T. Nakai, J.A. Montgomery Jr., J.E. Peralta, F. Ogliaro, M. Bearpark, J.J. Heyd, V. Brothers, K.N. Kudin, V.N. Staroverov, T. Keith, R. Kobayashi, J. Normand, K. Raghavachari, A. Rendell, J.C. Burant, S.S. Iyengar, J. Tomasi, M. Cossi, N. Rega, J.M. Millam, M. Klene, J.E. Knox, J.B. Cross, V. Bakken, C. Adamo, J. Jaramillo, R. Gomperts, R.E. Stratmann, O. Yazyev, A.J. Austin, R. Cammi, C. Pomelli, J.W. Ochterski, R.L. Martin, K. Morokuma, V.G. Zakrzewski, G.A. Voth, P. Salvador, J.J. Dannenberg, S. Dapprich, A.D. Daniels, O. Farkas, J.B. Foresman, J.V. Ortiz, J. Cioslowski and D.J. Fox, Gaussian 09, Revision B.01, Gaussian Inc., Wallingford, CT (2010).
30. C. Lee, W. Yang and R.G. Parr, *Phys. Rev. B*, **37**, 785 (1988); https://doi.org/10.1103/PhysRevB.37.785.
31. J.B. Foresman and A. Frisch, Exploring Chemistry with Electronic Structure Methods, Gaussian Inc., Pittsburgh, PA, edn 2 (1996).
32. L. Barbossa, Ph.D. Thesis, Theoretical Studies of Nitrile Hydrolysis by Solid Acid Catalyst, Technische Universiteit, Eindhoven, Netherlands (2000).
33. J.W. Ochterski, Thermochemistry in Gaussian (2000); http://www.gaussian.com/g_whitepap/thermo.htm.
34. H. Fu, Z.P. Liu, Z.H. Li, W.N. Wang and K.N. Fan, *J. Am. Chem. Soc.*, **128**, 11114 (2006); https://doi.org/10.1021/ja0611745.
35. N.H. Nguyen, T.H. Tran, M.T. Nguyen and M.C. Le, *Int. J. Quantum Chem.*, **110**, 2653 (2010); https://doi.org/10.1002/qua.22389.
36. J.S.O. Evans, J.C. Hanson and A.W. Sleight, *Acta Crystallogr.*, **54**, 705 (1998); https://doi.org/10.1107/S0108768198000962.
37. G.K. Chuah and S. Jaenicke, *Appl. Catal. A*, **163**, 261 (1997); https://doi.org/10.1016/S0926-860X(97)00103-8.
38. A. Khodakov, J. Yang, S. Su, E. Iglesia and A.T. Bell, *J. Catal.*, **177**, 343 (1998); https://doi.org/10.1006/jcat.1998.2143.
39. H. Mohebbi, T. Ebadzadeh and F.A. Hesari, *J. Power Sources*, **178**, 64 (2008); https://doi.org/10.1016/j.jpowsour.2007.12.054.